Automotive Innovation (2024) 7:271–282
https://doi.org/10.1007/s42154-023-00243-2

Efficient Cooperative Adaptive Cruise Control Including Platoon Kinematics

Xinjie Zhang[1] · Shuai Li[1] · Konghui Guo[1] · Xiaoxing Lv[1] · Tao Peng[1] · Yonggang Liu[2]

Received: 24 June 2022 / Accepted: 20 July 2023 / Published online: 6 April 2024

Abstract
Cooperative adaptive cruise control (CACC) is acknowledged as an efficient solution to relieve traffic congestion while ensuring traffic safety. This paper aims to improve traffic efficiency via both the effective following spacing policy and the CACC with platoon kinematics. Firstly, the correlation mechanism of safety spacing policy and time headway policy is analyzed, a versatile generic spacing model is established, and an efficient spacing policy is proposed by leveraging the concept of safety redundancy. Secondly, based on the "virtual centroid" of the platoon, the CACC upper control strategy with platoon kinematics is proposed to improve traffic efficiency. The strategy is complemented by the design of a sliding mode controller, which precisely allocates longitudinal acceleration. Additionally, a lower controller is developed to track the desired acceleration accurately and rapidly under various driving and braking conditions. Thirdly, eight typical scenarios for urban traffic are reconstructed via three-layer decompositions, and the index named synchronization is proposed to evaluate the performance of CACC with platoon kinematics. Finally, a simulation test is conducted, demonstrating that the proposed CACC strategy synchronously responds to the kinematics of the preceding platoon, reducing the accumulation of response delay, ensuring both vehicle following safety and efficiency.

Keywords CACC strategy · CACC evaluation · Efficient spacing policy · Generic spacing model · Platoon kinematics

1 Introduction

Traffic congestion and safety issues have been exacerbated by human driver errors and limitations. The development of adaptive cruise control (ACC) since the 1960s has significantly contributed to traffic safety and efficiency by enabling automatic following of the preceding vehicle, reducing driver effort [1]. To further enhance these aspects, the stop-and-go ACC and the cooperative adaptive cruise control (CACC) have been proposed [2].

CACC represents an enhancement of ACC that incorporates vehicle-to-vehicle (V2V) communication to utilize the rich information of the preceding vehicle and form platoon, improving road safety, reducing fuel consumption, and increasing traffic flow [3, 4]. Amoozadeh et al. [5] transmitted the preceding vehicle's acceleration and maximum deceleration to the host vehicle to design the longitudinal control of the platoon, meeting the requirements of safety and theoretical throughput. Rajamani et al. [6] introduced the lead and preceding vehicles' speed and acceleration to the host vehicle to design the longitudinal control of the National Automated Highway System Consortium (NAHSC) demonstration, realizing accurate speed tracking and spacing control. In addition, researchers have been trying to consider the information from every vehicle in platooning. Madeleine et al. [7] introduced unit-center-referenced formation and defined the "virtual leader" by averaging the positions of all vehicles in a two-vehicle platoon. Zhang et al. [8] proposed the "virtual centroid" of the platoon to describe the platoon kinematics considering all vehicles in front of the host vehicle, and thereby improving traffic efficiency. The CACC with its platoon kinematics demonstrates significant benefits and potential for enabling the host vehicle to respond promptly and reasonably, thereby improving overall traffic efficiency.

✉ Xinjie Zhang
x_jzhang@jlu.edu.cn

[1] State Key Laboratory of Automotive Simulation and Control, Jilin University, Changchun 130022, Jilin Province, People's Republic of China

[2] State Key Laboratory of Mechanical Transmission and College of Mechanical and Vehicle Engineering, Chongqing University, Chongqing, People's Republic of China

The spacing policy also plays an important role in improving traffic efficiency. Shladover et al. [9] studied a constant spacing policy of less than one meter to improve traffic capacity for close-formation platoons, which relied on a well-designed controller. The constant time headway policy was also applied to vehicle platoons to improve traffic efficiency by minimizing the values of time headway [10, 11]. Yanakiev et al. [12] proposed two nonlinear spacing policies, namely variable time headway and variable separation error gain, for automated heavy-duty vehicles platoon, leading to increased traffic throughput. In previous research, the integrated spacing policy was proposed to improve traffic efficiency by utilizing the safety redundancy [13]. The "virtual centroid" was proposed to describe platoon kinematics, and the control strategy was designed by combining the integrated spacing policy and virtual centroid, further improving traffic efficiency [8]. Both CACC with its platoon kinematics and spacing policy significantly influence traffic efficiency.

The CACC evaluation has also been under study. Tongue et al. [14] proposed the worst-case performance algorithm to evaluate the robustness of platoon controllers. Van et al. [3] utilized traffic throughput and roadway capacity to evaluate CACC's impact on traffic flow. Yang et al. [15] focused on CACC's fuel economy, while Li et al. [16] proposed time-exposed time-to-collision (TET) and time-integrated time-to-collision (TIT) to evaluate the safety of CACC. In 2019, the ISO 20035 defined the performance evaluation methods of the CACC system from the perspective of production and application, including detection range, lane and range discrimination, and cooperative operating modes/states switching, but it notes that the coordinated strategies to control groups of vehicles, such as platooning, are not within the scope of ISO 20035 [17]. The platooning and platoon kinematics are vital to CACC, whereas the evaluation methods for CACC with platoon kinematics are an important and opening problem to be solved.

To improve traffic efficiency and evaluate the CACC with platoon kinematics, this paper attempts to explore the correlation mechanisms between safety spacing policy and time headway policy, establish the efficient spacing policy and its hierarchical control, and propose the evaluation methodology for CACC with platoon kinematics. The main contributions are as follows:

- The correlation mechanism between the safety spacing policy and time headway policy is revealed and the generic spacing model is proposed to unify these two policies, and the logic operation based efficient spacing policy is proposed for vehicle following control, avoiding the real-time solve of the critical velocity and the complex switching law depending on the critical velocity.
- The evaluation methodology for CACC with platoon kinematics is proposed, in which eight typical scenarios are reconstructed via three-layer decompositions, and the CACC synchronic index is proposed to evaluate the CACC performance with platoon kinematics.
- The hierarchical control of CACC including platoon kinematics is presented, in which the upper controller with platoon kinematics, the lower controller with vehicle nonlinear and time-variable characteristics, are established to improve traffic efficiency.

The subsequent sections of this paper are organized as follows: Sect. 2 delves into the correlation mechanism between safety spacing policy and time headway policy and proposes the efficient spacing policy. Section 3 establishes the upper controller for CACC with platoon kinematics and the lower controller with vehicle nonlinear and time-variable characteristics. Section 4 proposes the evaluation methodology for CACC with platoon kinematics. Section 5 illustrates the simulation test, and Sect. 6 draws conclusions.

2 Efficient Spacing Policy

The safety spacing policy and constant time headway policy pivotal for vehicle following control, dictating the distance that the host vehicle needs to maintain from the preceding vehicle. In this section, the correlation mechanism of the safety spacing policy and time headway policy is studied, and the generic spacing model and the efficient spacing policy are proposed.

2.1 Generic Spacing Model

The braking process is assumed as an extreme case: the preceding vehicle with velocity v_{i-1} is at its maximum deceleration ($-a_{\mathrm{bmax}}$), while the host vehicle with velocity v_i is at its maximum acceleration ($a_{\max}$). The minimum centroid distance, $D_{\mathrm{min}i}$, ensuring the safety for the vehicle mass point model without geometric considerations, is expressed by Eq. (1). The detailed derivation is elucidated in Appendix A.

$$
\begin{aligned}
D_{\mathrm{min}i} &= S_i - S_{i-1} + d_{ai} \\
&= \frac{v_i^2 - v_{i-1}^2}{2a_{\mathrm{bmax}}} + [\tau_{11} + \tau_{12} + \tau_{21} + \frac{\tau_{22}}{2} \\
&+ \frac{a_{\max}}{a_{\mathrm{bmax}}}\left(\tau_{11} + \frac{\tau_{12}}{2}\right)]v_i - \frac{1}{24}a_{\mathrm{bmax}}\tau_{22}^2 \\
&+ a_{\max}[\frac{\tau_{11}^2}{2} + \tau_{11}\tau_{12} + \frac{1}{6}\tau_{12}^2 + \left(\tau_{11} + \frac{\tau_{12}}{2}\right)\left(\tau_{21} + \frac{\tau_{22}}{2}\right) \\
&+ \frac{a_{\max}}{2a_{\mathrm{bmax}}}\left(\tau_{11} + \frac{\tau_{12}}{2}\right)^2] + d_{ai}
\end{aligned} \tag{1}
$$

where τ_{11} is the time required to detect that the preceding vehicle starts to brake, τ_{12} is the time for the driver to release the accelerator pedal completely, τ_{21} is the time to move the foot to the braking pedal and eliminate the mechanical clearance of the braking system, τ_{22} is the time to increase braking force, τ_3 is the continuous braking time, τ_4 is the braking release time, and d_{ai} is a safety margin. It is worth noting that τ_{12} and τ_{21} are eliminated for CACC. For brevity, the last three terms of Eq. (1) are simplified into the static distance d_{min}, representing the centroid distance between the host vehicle and preceding vehicle when their velocities are 0.

According to Eq. (1), the spacing policy for emergency braking and the stable following are obtained:

(1) Emergency braking case

For an emergency braking case, it is assumed that a static vehicle or an obstacle suddenly appears in front of the host vehicle. At this moment, the velocity of the preceding target, $v_{i-1} = 0$, and the host vehicle travels with a constant velocity v_i, the safe distance of the emergency braking case d_{emei} is derived as

$$
d_{\mathrm{emei}} = \frac{v_i^2}{2a_{\mathrm{bmax}}} + v_i \cdot \left(\tau_{11} + \tau_{21} + \frac{\tau_{22}}{2}\right) + d_{\mathrm{min}} \tag{2}
$$

Equation (2) can avoid the collision in emergencies, and is defined as the safety spacing policy d_{safi},

$$
d_{\mathrm{safi}} = v_i\left(\frac{v_i}{2a_{\mathrm{bmax}}} + \tau\right) + d_{\mathrm{min}} \tag{3}
$$

where $\tau = \tau_{11} + \tau_{21} + \tau_{22}/2$.

(2) Steady following case

For a steady following case, the host vehicle and preceding vehicle have the same initial velocity v_i, and the safe distance of the steady following case d_{stei} is derived as

$$
d_{\mathrm{stei}} = v_i \cdot \left(\tau_{11} + \tau_{21} + \frac{\tau_{22}}{2} + \frac{a_{\max}}{a_{\mathrm{bmax}}}\tau_{11}\right) + d_{\mathrm{min}} \tag{4}
$$

And Eq. (4) is rewritten as the constant time headway policy d_{cthi},

$$
d_{\mathrm{cthi}} = v_i \cdot th + d_{\mathrm{min}} \tag{5}
$$

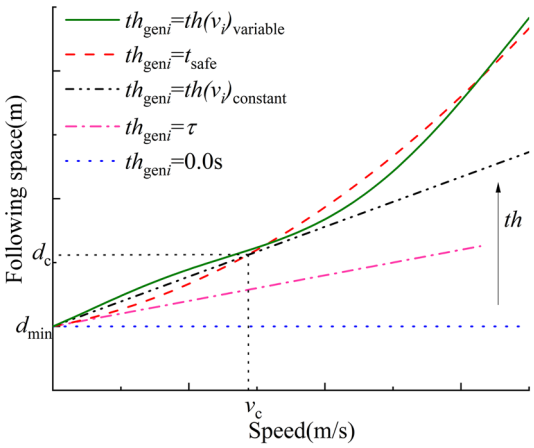

Fig. 1 The schematic diagram of generic spacing model

where $th = \tau_{11} + \tau_{21} + \frac{\tau_{22}}{2} + \frac{a_{\max}}{a_{\mathrm{bmax}}}\tau_{11} > \tau$.

Comparing Eqs. (3) and (5), it is shown that the safety spacing policy is a variable time headway policy and its time headway is $v_i/2a_{\mathrm{bmax}} + \tau$, which varies linearly with velocity. And Eqs. (3) and (5) are unified to the generic spacing model $d_{\mathrm{gen}i}$,

$$
\begin{aligned}
d_{\mathrm{gen}i} &= v_i \cdot th_{\mathrm{gen}i} + d_{\mathrm{min}} \\
th_{\mathrm{gen}i} &= \begin{cases} th(v_i), \text{time headway} \\ v_i/2a_{\mathrm{bmax}} + \tau, \text{safety spacing} \end{cases}
\end{aligned} \tag{6}
$$

where $th_{\mathrm{gen}i}$ is the time headway of the generic spacing model, $th(v_i)$ is the time headway at the current velocity v_i.

The generic spacing model, depicted schematically in Fig. 1, serves as a temporal headway policy that unifies both safety spacing and time headway policies. When the time headway of the generic spacing model $th_{\mathrm{gen}i}$ is a constant, the generic spacing model is the constant time headway policy shown as $th_{\mathrm{gen}i} = th(v_i)_{\mathrm{constant}}$, $th_{\mathrm{gen}i} = \tau$, and $th_{\mathrm{gen}i} = 0$s; when the $th_{\mathrm{gen}i}$ is variable, the generic spacing model is the variable time headway policy shown as $th(v_i)_{\mathrm{variable}}$ and t_{safe}. The t_{safe} is the safety spacing policy illustrated by the red long-dash line, and its tangent line's slope is just its time headway at each velocity. And the details are as follows.

- When $v_i = 0$, the generic spacing model's curves have the same starting point, $(0, d_{\mathrm{min}})$, representing that the distance between the host vehicle and preceding vehicle equals d_{min} when their velocities are 0. The tangent to the safety spacing policy is just the constant time headway curve with $th(v_i) = \tau$ indicated as the pink dot-dash line, which is a special case of the safety spacing policy. $th(v_i) = 0$ is the ideal boundary denoted by the blue dotted line,

meaning that the distance between the preceding and host vehicle is $d_{\min}$ at any speed, and the platoon travels in a train-like form, reaching maximum traffic density.

- When $v_i > 0$, the slope of the constant time headway curve (depicted by the black double-dotted-dash line) and the safety spacing curve changes monotonically with increasing vehicle velocity, and $th(v_i) > \tau$, so they only have one intersection (v_c, d_c) shown in Eq. (7). As shown in Fig. 1, when the vehicle velocity v_i surpasses the critical velocity v_c, the constant time headway policy exhibits reduced safety redundancy. Conversely, when v_i is less than v_c, the safety spacing policy manifests diminished safety redundancy. When v_i equals v_c, the two policies have the same safety redundancy, as detailed in a previous work on the integrated spacing policy [13]. It can be concluded that the safety spacing curve only has one intersection with the constant time headway curve when $th(v_i) > \tau$ and $v_i > 0$. And for the variable time headway curve, shown as the olive green solid line, its slope may not change monotonically with increasing vehicle velocity. Multiple intersections may exist for the time headway curve and the safety spacing curve, especially when the time headway is velocity-varying with higher-order functions or lacks an explicit function. The real-time determination of critical velocities, as required by the critical velocity-based switching law and spacing policy, faces challenges and limitations. Therefore, an efficient spacing policy for the generic spacing model demands further investigation.

$$\begin{cases} v_c = 2a_{\text{bmax}}\left(th(v_i) - \tau\right) \\ d_c = 2a_{\text{bmax}}\left(th(v_i) - \tau\right)th(v_i) + d_{\min} \end{cases} \tag{7}$$

where v_c is the critical velocity, and d_c is the distance between the preceding vehicle and host vehicle at critical velocity.

2.2 Efficient Spacing Policy Via Logic Operation

In this section, the author propose the efficient spacing policy via logic operation to get the generic spacing model's safety redundancy. The logic operation is adopted to compare the distances of the safety spacing and constant time headway policies, and the minimum one is set as the spacing policy. As for the generic spacing model, a shorter time headway th_{geni} has less safety redundancy, and the efficient spacing policy d_{efi} is derived as presented in Eq. (8), representing the distance from the ith vehicle to its preceding vehicle. This efficient spacing policy can make use of the safety redundancy of various spacing policies, avoiding the need for solving intersections and the complex switching law depending on the critical velocity, thereby extending its work range.

$$\begin{aligned} d_{\text{efi}} &= v_i \cdot \tau_{\text{efi}} + d_{\min} \\ \tau_{\text{efi}} &= \min\left\{ \frac{v_i}{2a_{\text{bmax}}} + \tau, th(v_i) \right\} \end{aligned} \tag{8}$$

3 CACC with Platoon Kinematics

In this section, the hierarchical control of CACC including platoon kinematics is established. The CACC upper control strategy with platoon kinematics is proposed to improve traffic efficiency, and its sliding mode controller is designed to allocate the longitudinal acceleration. Additionally, the lower controller, specialized for various driving and braking conditions, is developed to accurately and rapidly track the desired acceleration.

3.1 Hierarchical Control Framework

The hierarchical control framework in this paper is illustrated in Fig. 2. The upper controller, with platoon kinematics, allocates the host vehicle's desired acceleration; and the lower controller tracks the desired acceleration by regulating the throttle opening and brake pressure.

3.2 Upper Control Strategy

The upper control strategy is designed to allocate the desired distance and acceleration for each vehicle. In this section, the vehicle length is included in the presented efficient spacing policy for CACC. And it is assumed that

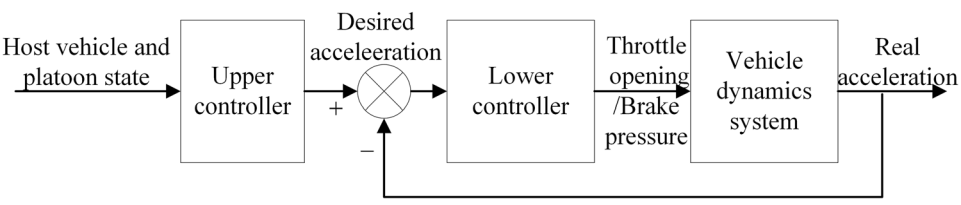

Fig. 2 The hierarchical control framework of CACC including platoon kinematics

the vehicles are homogeneous, and the information of the platoon is acquired by each vehicle without time delay.

In order to describe the platoon kinematics, the virtual centroid coordinates [8] for an n vehicles' platoon has been proposed as

$$\begin{aligned} d_{\mathrm{G}} &= \frac{\sum_{j=1}^{n-1} W_j d_n + \sum_{j=1}^{n-2} W_j d_{n-1} + \ldots + W_1 d_2}{\sum_{j=1}^{n} W_j} \\ v_{\mathrm{G}} &= \frac{\sum_{j=1}^{n} W_j v_j}{\sum_{j=1}^{n} W_j} \\ a_{\mathrm{G}} &= \frac{\sum_{j=1}^{n} W_j a_j}{\sum_{j=1}^{n} W_j} \end{aligned} \tag{9}$$

where d_{G}, v_{G}, and a_{G} are the distance, velocity, and acceleration of the virtual centroid, respectively, d_i is the centroid distance between the ith vehicle and its preceding vehicle, and W_j, v_j, and a_j are the weight, velocity, and acceleration of the jth vehicle in the platoon, respectively. The virtual centroid, representing the whole platoon motion state, is then introduced to the CACC to improve traffic efficiency.

First, the desired distance is obtained. To improve traffic efficiency, the switching law of the following target is proposed: when d_i falls below the lower threshold d_{l}, the ith vehicle's following target is the preceding vehicle; when d_i exceeds the upper threshold d_{u}, the following target is the virtual centroid; and when $d_{\mathrm{l}} \le d_i \le d_{\mathrm{u}}$, the ith vehicle keeps the current following target and desired distance to minimize frequent target switches [8]. Combining with this switching law, the efficient spacing policy considering vehicle length and platoon kinematics, $d_{\mathrm{des}i}$, is:

$$d_{\mathrm{des}i} = \begin{cases} v_i \cdot \tau_{\mathrm{ef}i} + d_{\min} + L, \ d_i < d_{\mathrm{l}} \\ \text{keep the current state}, \ d_{\mathrm{l}} \le d_i \le d_{\mathrm{u}} \\ \frac{\sum_{j=1}^{i-1} W_j (i-j)}{\sum_{j=1}^{i-1} W_j} \left(v_i \cdot \tau_{\mathrm{ef}i} + d_{\min} + L \right), d_i > d_{\mathrm{u}} \end{cases} \tag{10}$$

with

$$d_{\mathrm{l}} = k_{\mathrm{l}} \left(v_i \cdot \tau_{\mathrm{ef}i} + d_{\min} + L \right) \tag{11}$$

and

$$d_{\mathrm{u}} = k_{\mathrm{u}} \left(v_i \cdot \tau_{\mathrm{ef}i} + d_{\min} + L \right) \tag{12}$$

where $d_{\mathrm{des}i}$ is the desired centroid distance between the ith vehicle and following target, k_{l} and k_{u} are the lower threshold coefficient and upper threshold coefficient, respectively, which are tuned by experience, and L is the vehicle length.

Next, the vehicle longitudinal control is described as a first-order inertial system, as shown in Eq. (13). The centroid distance tracking error of the ith vehicle, e_i, is shown in Eq. (14), and the control objective is to regulate e_i and its derivative to zero. To achieve this objective, a sliding mode controller is designed to allocate the desired acceleration of the ith vehicle, the sliding surface is defined by Eq. (16), and the desired acceleration of the ith vehicle is solved through Eq. (17), referred to as the control input, as shown in Eq. (18).

$$\dot{a}_i = -\tfrac{1}{\widehat{\tau}_s} a_i + \tfrac{1}{\widehat{\tau}_s} a_{\mathrm{des}i} \tag{13}$$

$$e_i = d_{\mathrm{rea}i} - d_{\mathrm{des}i} \tag{14}$$

$$d_{\mathrm{rea}i} = x_{\mathrm{t}} - x_i \tag{15}$$

$$S = e_i + c\dot{e}_i, c > 0 \tag{16}$$

$$\dot{S} = -\lambda S, \lambda > 0 \tag{17}$$

$$a_{\mathrm{des}i} = \begin{cases} h_1 e_i + h_2 v_{\mathrm{t}} + h_3 v_i + h_4 a_i + h_5 a_{\mathrm{t}}, d_i < d_{\mathrm{l}} \\ \text{keep the current state}, d_{\mathrm{l}} \le d_i \le d_{\mathrm{u}} \\ h_1' e_i + h_2' v_{\mathrm{t}} + h_3' v_i + h_4' a_i + h_5' a_{\mathrm{t}}, d_i > d_{\mathrm{u}} \end{cases} \tag{18}$$

with

$$h_1 = \frac{\lambda \widehat{\tau}_s}{c\tau_{\mathrm{ef}i}}, h_2 = \frac{(\lambda c + 1)\widehat{\tau}_s}{c\tau_{\mathrm{ef}i}},$$

$$h_3 = \frac{-\left(\lambda c + 1 + \dot{\tau}_{\mathrm{ef}i} + \lambda c \dot{\tau}_{\mathrm{ef}i} + c\ddot{\tau}_{\mathrm{ef}i}\right)\widehat{\tau}_s}{c\tau_{\mathrm{ef}i}},$$

$$h_4 = 1 - \frac{\widehat{\tau}_s \left[(\lambda c + 1)\tau_{\mathrm{ef}i} + c + 2c\dot{\tau}_{\mathrm{ef}i}\right]}{c\tau_{\mathrm{ef}i}}, h_5 = \frac{\widehat{\tau}_s}{\tau_{\mathrm{ef}i}},$$

$$h_1' = \frac{\sum_{j=1}^{i-1} W_j}{\sum_{j=1}^{i-1} W_j (i-j)} \frac{\lambda \widehat{\tau}_s}{c\tau_{\mathrm{ef}i}},$$

$$h_2' = \frac{\sum_{j=1}^{i-1} W_j}{\sum_{j=1}^{i-1} W_j (i-j)} \frac{(\lambda c + 1)\widehat{\tau}_s}{c\tau_{\mathrm{ef}i}},$$

$$h_3' = \frac{-\sum_{j=1}^{i-1} W_j}{\sum_{j=1}^{i-1} W_j (i-j)} \frac{\left(\lambda c + 1 + \dot{\tau}_{\mathrm{ef}i} + \lambda c \dot{\tau}_{\mathrm{ef}i} + c\ddot{\tau}_{\mathrm{ef}i}\right)\widehat{\tau}_s}{c\tau_{\mathrm{ef}i}},$$

$$h_4' = 1 - \frac{\widehat{\tau}_s(\lambda c + 1)}{c} - \frac{\sum_{j=1}^{i-1} W_j}{\sum_{j=1}^{i-1} W_j (i-j)} \left[\frac{\widehat{\tau}_s \left(c + 2c\dot{\tau}_{\mathrm{ef}i}\right)}{c\tau_{\mathrm{ef}i}} \right],$$

Table 1 Control parameters

Symbol	Value
λ	1
c	1
$\widehat{\tau}_s$	0.3
W_j	$W_j = \begin{cases} \frac{1}{i-1} & j < i \\ 0 & j > i \end{cases}$

$$h_5' = \frac{\sum_{j=1}^{i-1} W_j}{\sum_{j=1}^{i-1} W_j (i-j)} \frac{\widehat{\tau}_s}{\tau_{\mathrm{ef}i}}$$

where x_t, v_t, and a_t are the position, velocity, and acceleration of following target separately, x_i is the real position of the ith vehicle, $d_{\mathrm{rea}i}$ is the real centroid distance between the ith vehicle and its following target, $\widehat{\tau}_s$ is the estimation of the vehicle response time.

The effects of the parameters on the upper control strategy are studied, including the sliding surface convergence speed, λ, sliding surface parameter, c, and weight of ith vehicle in the platoon, W_i. And it is shown that: first, λ and c mainly influence the transient performance of the controller, where larger λ and smaller c make the real distance converge to the desired distance faster; second, W_i mainly influences the prospective performance of the controller, with smaller weights for vehicles near the ith vehicle, resulting in diminished acceleration and velocity amplitudes for the ith vehicle. However, this comes at the expense of an increased tracking error with respect to its preceding vehicle. The choice of W_i necessitates a delicate balance to optimize performance. And the tuned values for the sliding mode controller parameters, determined through a trial-and-error process, are presented in Table 1.

String stability is important for the design of CACC system. Xiao et al. [18] designed a sliding model control law for the platoon, analyzed the negative effect of time delays on the homogeneous string stability, and obtained the string stable conditions. Specifically, the string stability could be ensured if the time headway h_i and communication time delay Δ_i met $h_i > 2\Delta_i$ and the sliding surface convergence speed fell within the range $\lambda_i \in [0, (h_i - 2\Delta_i)/2h_i\Delta_i]$. In this paper, $h_i = \tau_{\mathrm{ef}i} = 1.5\mathrm{s}$, $\lambda_i = 1$, and Δ_i is assumed as 0.3 s, and the relationship $h_i = 1.5\mathrm{s} > 2 \times 0.3\mathrm{s} = 2\Delta_i$, $\lambda_i = 1 \in [0, 1]$ are satisfied, showing that the proposed CACC can satisfy the string stability.

3.3 Lower Controller

In this section, the lower controller is established to track the desired acceleration, which is divided into braking and driving conditions. Achieving precise and rapid tracking of acceleration is imperative for ensuring following safety and string stability.

3.3.1 Driving Conditions Control

Here, the feedforward-feedback control is designed to control throttle opening during driving conditions to achieve accurate and swift tracking of the desired acceleration. To address the nonlinear and time-variable nature of the vehicle's longitudinal dynamics, stemming from components like the hydraulic torque converter, transmission, and main decelerator, a fuzzy PID controller is employed as the feedback control. This fuzzy PID controller adapts its parameter settings to effectively mitigate acceleration tracking errors.

As shown in Fig. 3, the inverse model of longitudinal dynamics computes the feedforward throttle opening $u_{\mathrm{throttle,f}}$, while the fuzzy PID controller calculates the feedback throttle opening $u_{\mathrm{throttle,b}}$, and the $u_{\mathrm{throttle,f}}$ and $u_{\mathrm{throttle,b}}$ constitute the throttle opening u_{throttle}. The control law for driving conditions is expressed as

$$\begin{aligned} u_{\mathrm{throttle}} =& f_\mathrm{e}^{-1}\left(T_{\mathrm{e,des}}, \omega_{\mathrm{e,des}}\right) + \left(K_{\mathrm{p,o}} + \Delta K_{\mathrm{p,r}}\right) e_\mathrm{a} \\ &+ \left(K_{\mathrm{i,o}} + \Delta K_{\mathrm{i,r}}\right) \cdot \int_0^t e_a \mathrm{d}t + \left(K_{\mathrm{d,o}} + \Delta K_{\mathrm{d,r}}\right) \frac{\mathrm{d}e_\mathrm{a}}{\mathrm{d}t} \end{aligned} \tag{19}$$

where f_e^{-1} is the inverse model of engine operating characteristics, $T_{\mathrm{e,des}}, \omega_{\mathrm{e,des}}$ are desired engine torque, desired engine speed, $K_{\mathrm{p,o}}, K_{\mathrm{i,o}}, K_{\mathrm{d,o}}$ are the proportional coefficient, integral coefficient, differential coefficient whose values are 0.03, 0.06 and 0 respectively, $\Delta K_{\mathrm{p,r}}, \Delta K_{\mathrm{i,r}}, \Delta K_{\mathrm{d,r}}$ are the actual parameter correction values of proportional, integral, and differential coefficient, e_a is the acceleration tracking error.

3.3.2 Braking Conditions Control

In the braking conditions, a feedforward-feedback control mechanism is formulated. Depicted in Fig. 4, the inverse model of vehicle longitudinal dynamics computes the feedforward brake master cylinder pressure $u_{\mathrm{b,f}}$, the PID controller calculates the feedback brake master cylinder pressure $u_{\mathrm{b,b}}$ to eliminate acceleration tracking errors, and the $u_{\mathrm{b,f}}$ and $u_{\mathrm{b,b}}$ constitute the brake master cylinder pressure u_b. The control law for braking conditions is expressed as

$$u_\mathrm{b} = \frac{T_{\mathrm{t,des}} - T_{\mathrm{t,e}}}{K_\mathrm{b}} + K_{\mathrm{p,b}} e_\mathrm{a} + K_{\mathrm{i,b}} \int_0^t e_\mathrm{a} \mathrm{d}t + K_{\mathrm{d,b}} \frac{\mathrm{d}e_\mathrm{a}}{\mathrm{d}t} \tag{20}$$

where $T_{\mathrm{t,des}}, T_{\mathrm{t,e}}$ are the desired engine torques and actual engine torques acting on the driving wheels, K_b is the proportional coefficient of braking torque and brake master cylinder pressure,$K_{\mathrm{p,b}}, K_{\mathrm{i,b}}, K_{\mathrm{d,b}}$ are the proportional, integral,

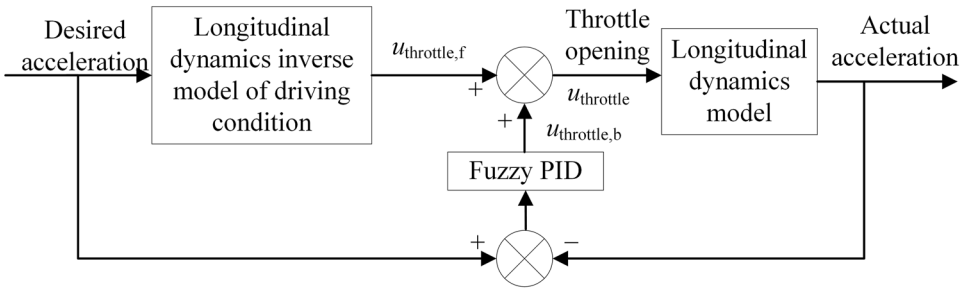

Fig. 3 The lower control diagram for driving conditions

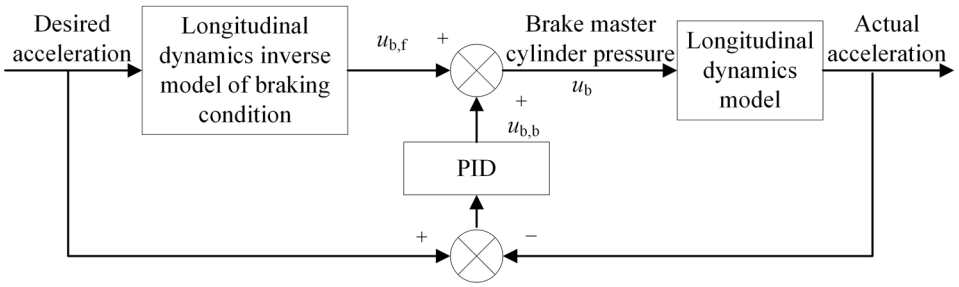

Fig. 4 The lower control diagram for braking conditions

and differential coefficient whose values are 0.5, 0.2, and 0, respectively.

3.3.3 Validation of Lower Control

The lower controller's effectiveness is assessed through simulation in an urban scenario, specifically focusing on the 130-390 s segment of the Worldwide Harmonized Light-duty Test Cycle (WLTC), marked by the red dash line in Fig. 5(a). As depicted in Fig. 5, the controller adeptly tracks the reference speed and acceleration demonstrating smooth and rapid responses. The root-mean-square of the speed tracking error is 0.16 m/s, and the root-mean-square of acceleration tracking error is 0.10 m/s^2. These results affirm that the presented lower controller can accurately and swiftly track the reference speed and acceleration in urban conditions.

4 Evaluation on CACC with Platoon Kinematics

In this section, eight simulation scenarios are reconstructed, and the CACC synchronic index is defined to evaluate the CACC performance with platoon kinematics.

4.1 Scenarios Re-construction

To systematize the urban traffic scene, eight typical scenarios are reconstructed using a three-layer decomposition, outlined in Table 2. From a macro perspective, these urban traffic scenarios can be categorized into two types based on the sources of disturbance.

(1) Disturbance inside the platoon

When the disturbance is inside the platoon, the scenarios are divided into the steady following and vehicle cut-out scenarios. (a) The steady following scenario

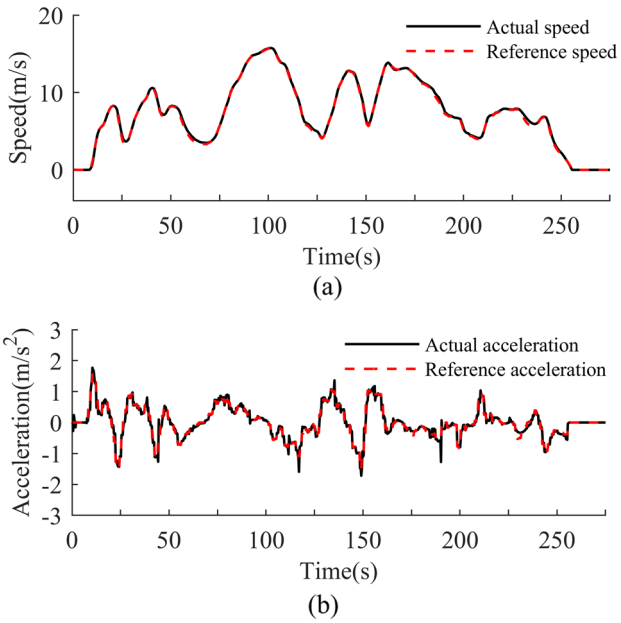

Fig. 5 Simulation results of lower control under WLTC

Table 2 Reconstructed scenarios

Level 1	Level 2	Level 3
Disturbance inside platoon	Steady following	Steady following
	Vehicle cut out	Vehicle cut out
Disturbance outside platoon	Moving vehicles appear in front of the platoon	Approaching a low-speed vehicle
		Keeping away from a low-speed vehicle
		Keeping away from a high-speed vehicle
	Static disturbance appears in front of the platoon	Approaching a static disturbance
		Emergency braking
	Vehicle cut in	Vehicle cut in

evaluates precision of following the preceding vehicle under steady conditions; and (b) the vehicle cut-out scenario assesses the safety of the process when a vehicle cuts out and subsequently re-establishes steady following.

(2) Disturbance outside the platoon

When the disturbance is outside the platoon, the scenarios are divided into three kinds of scenarios based on the state of the disturbance.

The first scenario is a moving vehicle appears in front of the platoon. These scenarios are divided into three cases according to the vehicle speed and its initial distance from the platoon: (a) Approaching a low-speed vehicle. (b) Keeping away from a low-speed vehicle. (c) Keeping away from a high-speed vehicle. The above three cases are used to evaluate the safety of processes that the high-speed platoon is reconstructed into the low-speed platoon when a low-speed vehicle appears with a safe distance; the high-speed platoon is reconstructed into the low-speed platoon when a low-speed vehicle appears less than the safety distance; the low-speed platoon is reconstructed into the high-speed platoon when a high-speed vehicle appears less than the safety distance.

The second scenario is a static disturbance that appears in front of the platoon, and these scenarios are divided into two cases according to the initial distance: (a) Approaching a static disturbance and (b) Emergency braking. The above two cases evaluate the safety of the platoon when decelerating to a stop via normal or emergency braking, respectively.

And the third scenario is vehicle cut-in, which is used to evaluate the process's safety from a vehicle cutting in to re-establishing steady following.

4.2 Evaluation Index

To evaluate response speeds of vehicle platoon with different lengths uniformly, the CACC synchronic index is proposed and defined as

$$I_{\mathrm{s}} = \frac{T_m - T_n}{m-n} \tag{21}$$

where T_n is the moment when the nth vehicle starts to change state, T_m is the moment when the mth vehicle starts its response, and $m > n$. The synchronic index shows the CACC's ability to make promoting control and agile response according to the platoon kinematics. A smaller I_{s} indicates improved synchronization and foresight within the vehicle platoon, leading to reduced response delay accumulation.

5 Simulation and Discussion

In this section, an urban stop-and-go case simulation test is studied to validate and evaluate the proposed CACC including platoon kinematics. A virtual test platform is developed via co-simulation with Matlab/Simulink and CarSim, considering a platoon with four vehicles. The CACC upper control strategy with platoon kinematics for stop-and-go (C-S&G) is expressed as the Eq. (17). The traditional ACC upper control strategy for stop-and-go (S&G) is represented by Eq. (22) [19]. The details of the lower controller are discussed in Sect. 3, and four SUVs are chosen as the test platoon using CarSim.

$$a_{i,\mathrm{des}} = \frac{1}{th} e_i + \frac{1}{th}\left(v_{i-1} - v_i\right) \tag{22}$$

The steady following scenario is selected as the simulation condition. The initial speed of the four vehicles is zero, and the initial distance from the front of the ith vehicle to the rear of its preceding vehicle is 2 m. The first vehicle travels at the reference speed, as shown by the solid blue line in Fig. 6. It stops completely during 0–5 seconds, then accelerates from 0 to 15 m/s, in ten seconds, maintains a constant speed during 15–25 seconds, and eventually decelerates to 0 in 10 s, and stops completely to the end. This scenario mainly studies the motion state of the rear three vehicles and verifies the tracking accuracy during steady following of the preceding vehicle. Table 3 shows the controller parameters. The simulation results of the steady following scenario are

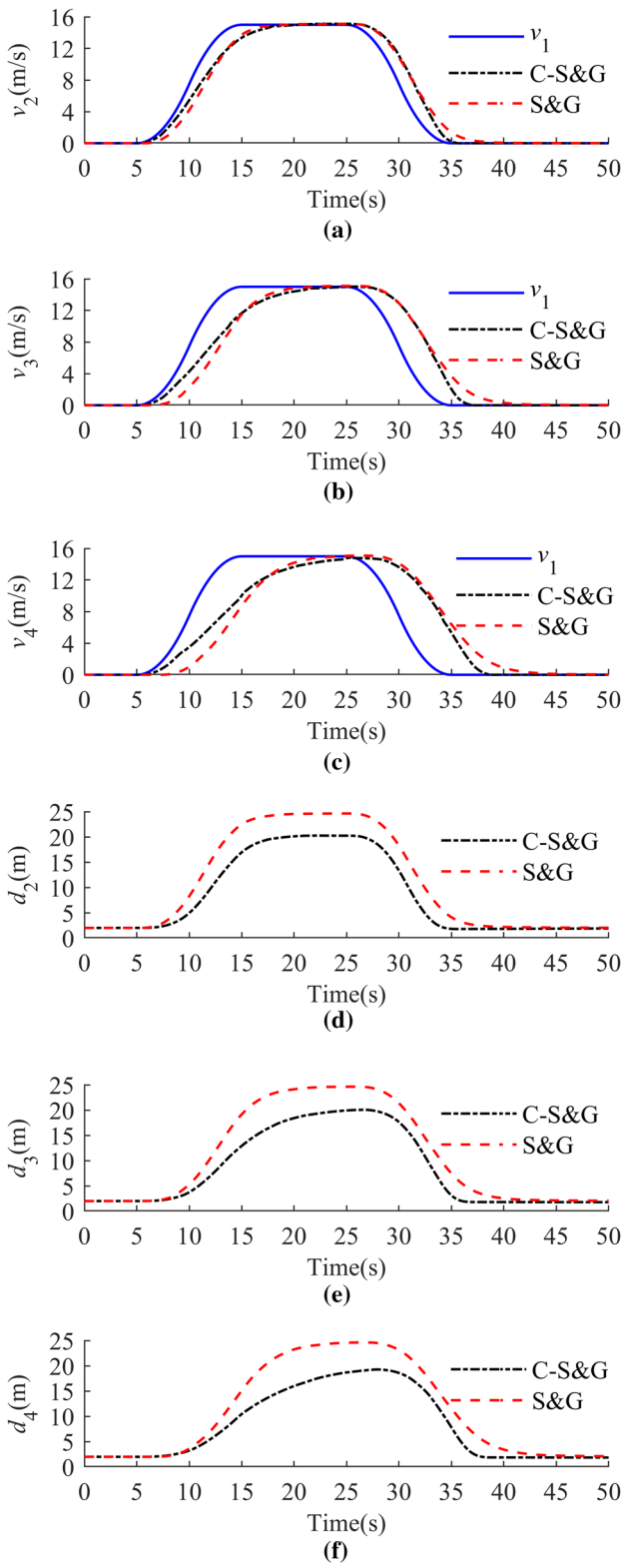

Fig. 6 Velocity and distance histories of the following vehicles in platoon

Table 3 Control parameters

Parameter name	Symbol	Value	Unit
Time headway on v_i	th(v_i)	1.5	s
Static distance	$d_{\min}$	2	m
Vehicle length	L	5	m
Minimum deceleration	a_{bmax}	− 7.5	m/s^2
Maximum acceleration	$a_{\max}$	3	m/s^2
Upper threshold coefficient	k_{u}	1	–
Lower threshold coefficient	k_{l}	0.9	–
Vehicle response time	τ_{s}	0.3	s
Braking response time	τ	0.2	s

Table 4 Simulation result of CACC synchronization

	T_1	T_2	T_3	T_4	I_{S}
C-S&G	5.00 s	5.15 s	5.26 s	5.36 s	0.12 s
S&G	5.00 s	5.66 s	6.58 s	7.33 s	0.78 s

depicted in Fig. 6, where the black dotted-dash line represents the presented CACC for S&G (C-S&G), and the red dash line represents the traditional ACC for S&G (S&G). The velocity histories of the second, third, and fourth vehicles are shown in Fig. 6(a)–(c), the distance histories of the second, third, and fourth vehicles to their preceding vehicles are shown in Fig. 6(d)–(f), and the CACC synchronic index is presented in Table 4. The simulation results demonstrate that:

- As shown in Fig. 6(d)–(f), both C-S&G and S&G ensure safety, with C-S&G exhibiting a smaller following distance compared to S&G. The average distance of C-S&G is 8.1 m less than S&G, indicating an enhancement in traffic efficiency and capacity.
- Figure 6 illustrates that C-S&G responds more accurately and rapidly to the state of the first vehicle compared to S&G, showcasing the foresightedness of the proposed C-S&G.
- As per Table 4, both the first vehicle of C-S&G and S&G starts at 5.00 s, the second vehicle of C-S&G starts at 5.15 s, the third vehicle of C-S&G responds to the first two vehicles in 0.26 s, the fourth vehicle responds to the first three vehicles in 0.36 s, and the fourth vehicle starts even faster than the second vehicle of S&G, which starts at 5.66 s. The C-S&G's synchronic index I_{S} is 85% lower than S&G's, showing that the platoon kinematics can reduce the response delay, and the presented C-S&G exhibits superior synchronization. The proposed CACC synchronic index effectively reveals the synchronic ability of the CACC with platoon kinematics.

In summary, the proposed CACC, including platoon kinematics, demonstrates superior foresight and synchronization compared to traditional ACC, thereby improving traffic efficiency.

6 Conclusion

An efficient cooperative adaptive cruise control including platoon kinematics is presented in this paper, in which the efficient spacing policy is proposed via the presented generic spacing model, the CACC strategy considering platoon kinematics and its evaluation methodology are proposed and studied.

The safety spacing policy is essentially a variable time headway policy whose time headway varies linearly with velocity. The generic spacing model unifies safety spacing and time headway policies, offering a flexible variable time headway policy. The efficient spacing policy is devised through logical operations, leveraging safety redundancy from various spacing policies and avoiding the critical velocity solving and complex switching laws.

The hierarchical control of CACC with platoon kinematics is presented, featuring an upper controller with platoon kinematics for improved traffic efficiency and a sliding mode controller for acceleration allocation. The lower controller manages driving and braking conditions, ensuring accurate and fast tracking of desired acceleration.

The CACC synchronic index and eight typical scenarios are proposed for comprehensive evaluation. A steady following scenario is simulated, demonstrating that the proposed CACC with platoon kinematics enhances traffic efficiency. The evaluation methodology proves effective in assessing the synchronic ability of the CACC with platoon kinematics.

Future work needs to extend the research to heterogeneous platoons, considering real-world vehicle tests and accounting for communication time delays.

Appendix A

The detailed derivation of Eq. (1):

In the extreme manual braking case, the host vehicle travels at constant acceleration $a_{\max}$, and its preceding vehicle travels at constant deceleration a_{bmax}, the braking process can be described by Figs. A1 and A2.

τ_{11} is the time required to detect that the preceding vehicle starts to brake, τ_{12} is the time for the driver to release the accelerator pedal completely; τ_{21} is the time to move the foot to the braking pedal and eliminate the mechanical clearance of the braking system, τ_{22} is the time to increase braking force, τ_3 is the continuous braking time, and τ_4 is the braking release time.

During the period of τ_{11}, the host vehicle travels at a uniform acceleration, so the distance and velocity is derived as:

$$s_{10} = v_i\tau_{11} + \tfrac{1}{2}a_{\max}\tau_{11}^2 \tag{A1}$$

$$v_1 = v_i + a_{\max}\tau_{11} \tag{A2}$$

During the period of τ_{12}, it is assumed that the acceleration decreases linearly, so the velocity and distance are calculated through integration:

$$v_2 = v_1 + \tfrac{1}{2}\tau_{12}a_{\max} \tag{A3}$$

$$s_{11} = v_1\tau_{12} + \tfrac{1}{6}a_{\max}\tau_{12}^2 \tag{A4}$$

During the period of τ_{21}, the vehicle travels at constant speed v_2:

$$s_{20} = v_2\tau_{21} \tag{A5}$$

During the period of τ_{22}, it is assumed the deceleration increases linearly, the velocity and distance are calculated through integration:

$$v_3 = v_2 - \tfrac{1}{2}a_{\text{bmax}}\tau_{22} \tag{A6}$$

$$s_{21} = v_2\tau_{22} - \tfrac{1}{6}a_{\text{bmax}}\tau_{22}^2 \tag{A7}$$

During the period of τ_3, the host vehicle travels at a uniform deceleration, so the distance and velocity is derived as:

$$s_3 = \tfrac{v_3^2}{2a_{\text{bmax}}} \tag{A8}$$

Above all, the braking distance of the host vehicle is:

$$S_i = s_{10} + s_{11} + s_{20} + s_{21} + s_3 \tag{A9}$$

Since the preceding vehicle travels at a uniform deceleration, the braking distance is derived as:

$$S_{i-1} = \tfrac{v_{i-1}^2}{2a_{\text{bmax}}} \tag{A10}$$

To guarantee the safety, the distance that the host vehicle should maintain from the preceding vehicle is:

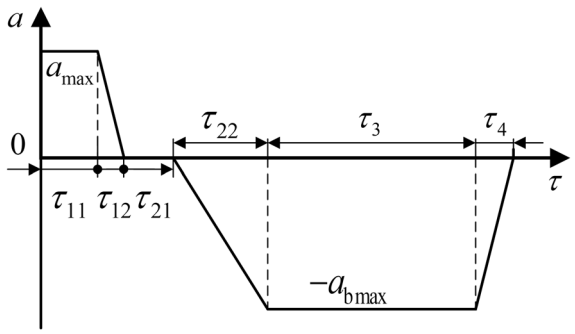

Fig. A1 The braking process of the ith vehicle

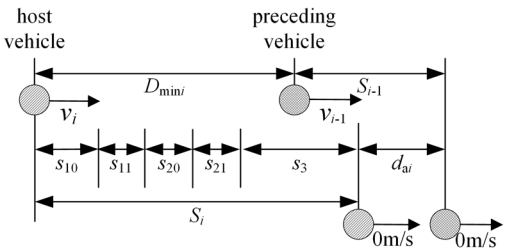

Fig. A2 The position of the ith vehicle during braking process

$$
\begin{aligned}
D_{\mathrm{mini}} = S_i - S_{i-1} + d_{ai} = \frac{v_i^2 - v_{i-1}^2}{2a_{\mathrm{bmax}}} + \Big[\tau_{11} + \tau_{12} + \tau_{21} + \frac{\tau_{22}}{2} \\
+ \frac{a_{\max}}{a_{\mathrm{bmax}}}\Big(\tau_{11} + \frac{\tau_{12}}{2}\Big)\Big] v_i - \frac{1}{24} a_{\mathrm{bmax}} \tau_{22}^2 \\
+ a_{\max}\left[\frac{\tau_{11}^2}{2} + \tau_{11}\tau_{12} + \frac{1}{6}\tau_{12}^2 + \Big(\tau_{11} + \frac{\tau_{12}}{2}\Big)\Big(\tau_{21} + \frac{\tau_{22}}{2}\Big)\right. \\
\left. + \frac{a_{\max}}{2a_{\mathrm{bmax}}}\Big(\tau_{11} + \frac{\tau_{12}}{2}\Big)^2\right] + d_{ai}
\end{aligned}
\tag{A11}
$$

where d_{ai} is a safety margin.

Appendix B: Description of parameters

a_{bmax}	Maximum deceleration (m/s^2)
$a_{\max}$	Maximum acceleration (m/s^2)
τ_{11}	Time to detect that the preceding vehicle starts to brake (s)
τ_{12}	Time for driver to release the accelerator pedal completely (s)
τ_{21}	Time to move the foot to the braking pedal and eliminate the mechanical clearance (s)
τ_{22}	Time to increase braking force (s)
τ_3	Continuous braking time (s)
τ_4	Braking force release time (s)
$d_{\min}$	Centroid distance between the host vehicle and preceding vehicle when their velocities are 0 (m)
th	Constant time headway (s)
v_i	Velocity of the ith vehicle (m/s)
d_{emei}	Safe distance of the emergency braking case (m)
d_{stei}	Safe distance of the steady following case (m)
d_{safi}	Safe distance of the safety spacing policy (m)
th_{geni}	Time headway of the generic spacing model (s)
$th(v_i)$	Time headway on v_i (s)
t_{safe}	Time headway of the safety spacing policy (s)
v_{c}	Critical velocity (m/s)
d_{efi}	Distance from the ith vehicle to its preceding vehicle of the efficient spacing policy (m)
d_i	Centroid distance between the ith vehicle and its preceding vehicle ((m))
e_i	Centroid distance tracking error of the ith vehicle (m)
d_{G}	Distance of the virtual centroid (m)
v_{G}	Velocity of the virtual centroid (m/s)
a_{G}	Acceleration of the virtual centroid (m/s^2)
d_{desi}	Desired centroid distance between the ith vehicle and following target (m)
a_{desi}	Desired acceleration of the ith vehicle (m/s^2)
λ	Sliding surface convergence speed
c	Sliding surface parameter
$\widehat{\tau}_s$	Estimation of the vehicle response time
W_i	Weight of ith vehicle in the platoon
u_{throttle}	Throttle opening
u_{b}	Brake master cylinder pressure
I_{s}	CACC Synchronic index (s)
τ_s	Vehicle response time (s)
τ	Braking response time (s)
$a_{i,\mathrm{des}}$	Desired acceleration of the ith vehicle for ACC (m/s^2)

Acknowledgements Special thanks are due to the National Natural Science Foundation of China (52072144, 52122216, 51675217), and the Opening Founding of State Key Laboratory of Automotive Simulation and Control (20201101) for supporting authors' research.

Declarations

Conflict of interest On behalf of all the authors, the corresponding author states that there is no conflict of interest.

References

1. Levine, W.S., Athans, M.: On the optimal error regulation of a string of moving vehicles. IEEE Trans. Automat. Contr. **11**(3), 355–361 (1966)
2. Xiao, L., Gao, F.: A comprehensive review of the development of adaptive cruise control systems. Veh. Syst. Dyn. **48**(10), 1167–1192 (2010)

3. Van Arem, B., Van Driel, C.J.G.: The impact of cooperative adaptive cruise control on traffic-flow characteristics. IEEE Trans. Intell. Transp. Syst. **7**(4), 429–436 (2006)
4. Montanaro, U., Dixit, S., Fallah, S., et al.: Towards connected autonomous driving: review of use-cases. Veh. Syst. Dyn. **57**(6), 779–814 (2019)
5. Amoozadeh, M., Deng, H., Chuah, C.N., et al.: Platoon management with cooperative adaptive cruise control enabled by VANET. Veh. Commun. **2**(2), 110–123 (2015)
6. Rajamani, R., Tan, H.S., Law, B.K., et al.: Demonstration of integrated longitudinal and lateral control for the operation of automated vehicles in platoons. IEEE Trans. Control Syst. Technol. **8**(4), 695–708 (2000)
7. Madeleine, E.L.Z., Dafflon, B., Gechter, F., et al.: Vehicle platoon control with multi-configuration ability. Procedia Comput. Sci. **9**, 1503–1512 (2012)
8. Zhang X, Li W, Guo K, et al.: Longitudinal acceleration allocation for cooperative adaptive cruise control including platoon kinematics. In: 2019 IEEE 28th International Symposium on Industrial Electronics (ISIE), pp. 1512-1517. Vancouver (2019)
9. Shladover, S.E.: Longitudinal control of automotive vehicles in close-formation platoons. J. Dyn. Syst. Meas. Control. **113**, 231–241 (1991)
10. Marsden, G., McDonald, M., Brackstone, M.: Towards an understanding of adaptive cruise control. Transp. Res. Part C Emerg. Technol. **9**(1), 33–51 (2001)
11. Ploeg J, van de Wouw N, Nijmeijer H.: Fault tolerance of cooperative vehicle platoons subject to communication delay. In: Proceedings of the 12th IFAC Workshop on Time Delay Systems (TDS 2015), Ann Arbor, MI, United States, 28–30 Jun 2015, pp. 352–357 (2015)
12. Yanakiev, D., Kanellakopoulos, I.: Nonlinear spacing policies for automated heavy-duty vehicles. IEEE Trans. Veh. Technol. **47**(4), 1365–1377 (1998)
13. Zhang, X., Huang, Y., Guo, K., et al.: Integrated spacing policy considering micro-and macroscopic characteristics. Automot. Innov. **2**(2), 102–109 (2019)
14. Tongue, B.H., Packard, A.K., Sachi, P.: An approach to determining worst case platoon behavior. Veh. Syst. Dyn. **28**(6), 357–383 (1997)
15. Yang, H., Rakha, H., Ala, M.V.: Eco-cooperative adaptive cruise control at signalized intersections considering queue effects. IEEE Trans. Intell. Transp. Syst. **18**(6), 1575–1585 (2016)
16. Li, Y., Wang, H., Wang, W., et al.: Evaluation of the impacts of cooperative adaptive cruise control on reducing rear-end collision risks on freeways. Accid. Anal. Prev. **98**, 87–95 (2017)
17. International Organization for Standardization: ISO 20035:2019 - Intelligent transport systems Cooperative adaptive cruise control systems (CACC) Performance requirements and test procedures (2019)
18. Xiao, L., Gao, F.: Practical string stability of platoon of adaptive cruise control vehicles. IEEE Trans. Intell. Transp. Syst. **12**(4), 1184–1194 (2011)
19. Zhou, J., Peng, H.: String stability conditions of adaptive cruise control algorithms. IFAC Proc. Vol. **37**(22), 649–654 (2004)